Fluctuation analysis of tension-controlled undulation forces between giant vesicles and solid substrates

Joachim O. Rädler, Toni J. Feder, Helmut H. Strey, and Erich Sackmann
Biophysics Group E22, Technical University of Munich, Garching, Germany
(Received 18 July 1994)

Using reflection interference contrast microscopy, we studied the thermal fluctuations of giant vesicles that weakly adhere to flat solid substrates. The absolute membrane-substrate separation distance was imaged and the average contact contour, including the contact area, the contact rounding, and the asymptotic contact angle, was determined. The static fluctuations in the flat, adhering part of the vesicle were analyzed. The spectrum of mean square amplitudes yielded the lateral membrane tension and the second derivative of the interaction potential. The vertical roughness and lateral correlation length were measured from the spatial autocorrelation of the undulations. The roughness was shown to obey the behavior predicted by functional renormalization in the observed tension regime of 10^{-6} to 10^{-4} J/m^2. Moreover, the measured separation distances can be explained within the framework of undulation and van der Waals forces and confirmed the model of tension-induced adhesion. However, the adhesion energies as well as the measured separation distances exhibit a weaker dependence on the membrane tension than predicted.

PACS number(s): 68.10.−m, 68.45.Kg, 42.30.−d

INTRODUCTION

During the last decade the physics of lipid membranes has received much attention. The wide interest in this field is due to the many different functions membranes fulfill in biology, and to the fact that they belong to the class of soft interfaces such as occur in microemulsions, liquid crystals, and polymer systems.

The original idea of Helfrich that soft membranes exhibit steric interactions stimulated the exploration of the statistical physics of membranes [1]. Membranes tend to repel each other by their thermal out-of-plane fluctuations in a way similar to the steric polymer interaction. In the course of more detailed theoretical studies in this field, universal scaling behavior as well as new phase transitions and complex phase diagrams were predicted [2]. Distinctions have to be made regarding whether a membrane is fluid, i.e., allowing lateral diffusion of its components, or is tethered, i.e., exhibiting shear elasticity through in-plane bonding. In this article we are concerned with the fluctuation-controlled interaction of fluid membranes with solid substrates.

Membrane systems that are accessible for experimental studies include liposomes and vesicles, microemulsions, lamellar liquid crystals, substrate supported membranes, and biological cells such as red blood cells [3]. The first indications for a steric interaction came from optical microscopy studies of fluid membranes, where membranes in multilamellar structures are found to repel each other [4]. The analysis of the observable thermal fluctuations of vesicles, also called "flickering," showed agreement with the model of thermally excited fluctuations and allowed high precision measurements of the bending moduli of lecithin membranes [5–8]. Careful small angle x-ray studies on the dilution of lamellar liquid crystals by increasing the water content showed furthermore that the distance versus bulk compressibility data were in good quantitative agreement with the steric force law derived by Helfrich [9].

The fluctuation-induced repulsion plays an important part in stabilizing vesicle suspensions. van der Waals (vdW) attraction is often overcome by the undulation force for membranes composed of neutral lipids in nonionic solutions. On the other hand, vesicles under tension adhere to each other due to the suppression of the fluctuation-induced force [10]. Evans and co-workers used the micropipette technique to measure the adhesion energy under controlled tension [11]. The model of tension-induced adhesion, however, was found to be difficult to prove quantitatively. Measurements of the contact angle between adhering vesicles reveal a remarkable constancy of the contact angle over a wide range of vesicle tensions that cannot be explained in terms of vdW and steric interaction [10,12]. This discrepancy also led to the hypothesis of a hidden microroughness [10].

In this article we apply reflection interference contrast microscopy (RICM) to investigate the weak interaction of giant phosphatidylcholine vesicles with flat substrates. With this interferometric technique vesicles are observed with monochromatic light incident and reflected from below. The interference micrographs exhibit Newton interference fringes that allow determination of the membrane-substrate separation distance [13]. We measured the vesicle area in contact with the substrate and its contour at the edge of the contact area. By analyzing sequences of momentary height profiles of the part of the vesicle adjacent to the flat substrate, the two-dimensional spatial spectrum of the out-of-plane fluctuations of the membrane was obtained. From the mean square amplitudes of the fluctuations, the membrane tension and the second derivative of the interaction potential were measured. The vertical roughness and the lateral correlation

length of the undulations can also be obtained directly from the autocorrelation function.

It was found that the tension measured from the fluctuation spectrum was in agreement with the measured roughness behavior that exhibited a logarithmic dependence as a function of the separation distance. The measured separation distances can be explained by superposition of the undulation forces of membranes under tension with the vdW attraction. However, the functional dependence of the separation distance seems to be weaker than predicted by the simple superposition model. The adhesion energies can be calculated by the Young-Dupre equation using the observed contact angles and measured tensions. A quadratic dependence of the adhesion energy on the membrane tension is found.

In summary, our technique allows us to measure six parameters of an adhering vesicle independently, i.e., the membrane tension, the harmonic approximation of the interaction potential (or alternatively the lateral correlation length $\xi_{\parallel}$ and the vertical roughness amplitude $\xi_{\perp}$) of the thermal membrane undulations, as well as the membrane-substrate separation distance, the contact angle, the diameter of the vesicle, and the diameter of the adhesion area.

THEORETICAL BACKGROUND

The statistical physics of membranes has been reviewed in several articles [2]. In this theoretical section we limit ourselves to the physics of one fluid membrane interacting with a flat solid substrate. First we consider the static fluctuation spectrum of an idealized "piece of membrane" in an attractive wall potential. We then describe the effective interaction potential between the membrane and the substrate by the superposition of the steric interaction of a membrane with a hard wall and the van der Waals attraction. In the last section we discuss the adhesion of giant vesicles to a substrate. Closed membranes are subject to topological constraints that lead to new boundary conditions and defined shapes [14]. However, the fluctuations of the flat part of the vesicle adjacent to the substrate can be approximately described by the equations derived for infinite membranes.

Static frequency spectrum of fluid membranes

Figure 1 depicts an oriented flat piece of membrane above a substrate. The membrane contour is described by the distance $s(\mathbf{x})$ from the substrate to the membrane perpendicular to the in-plane vector $\mathbf{x}=(x_1,x_2)$ (the so-called Monge representation). In the following we are concerned with the thermally driven undulations around the mean separation distance. We denote the local displacement amplitudes $h(\mathbf{x})=s(\mathbf{x})-\langle s(\mathbf{x})\rangle_t$. If an arbitrary observation area $A=L^2$ is chosen the undulations can be decomposed into discrete Fourier components defined by

$$h(\mathbf{x})=\sum_{\mathbf{q}} h_{\mathbf{q}} e^{i\mathbf{q}\mathbf{x}} ,$$
$$h_{\mathbf{q}}=\frac{1}{L^2}\int d^2\mathbf{x}\, h(\mathbf{x}) e^{-i\mathbf{q}\mathbf{x}} . \quad (1)$$

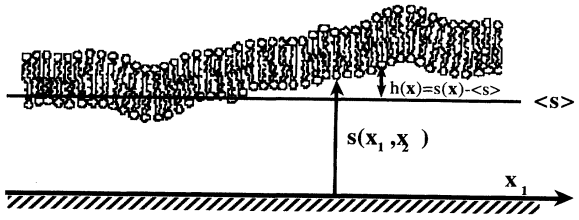

FIG. 1. Schematic diagram of a soft lipid membrane over a solid substrate. The membrane contour is described by its substrate-membrane separation distance $s(x)$. The amplitudes of the undulations about the mean position are denoted by $h(x)$. Thermal fluctuations lead to a repulsive steric interaction.

The magnitudes of the wave vector $\mathbf{q}=(q_{x_1},q_{x_2})$ takes values $2\pi/L(k,l)$, with k,l integers and $h_{\mathbf{q}}=h^*_{-\mathbf{q}}$, since $h(\mathbf{x})$ is real.

The free energy of the system is comprised of the elastic curvature energy, the surface tension energy, and the direct substrate-membrane interaction. The total free energy reads

$$F(h(\mathbf{x}))=\int d^2\mathbf{x}\{\tfrac{1}{2}K_c(\nabla^2 h)^2+\tfrac{1}{2}\sigma(\nabla h)^2+V(h)\} , \quad (2)$$

where K_c is the bending modulus, σ the membrane tension, and $V(h)$ the interaction potential. It is convenient to replace the interaction potential by its harmonic approximation $\frac{1}{2}V''=(\partial^2/\partial h^2)V_{h=0}$ around the mean membrane-wall separation distance $\langle s(\mathbf{x})\rangle$. This harmonic approximation is justified later.

Inserting expansion Eq. (1) into Eq. (2) yields for the free energy

$$F(h_q)=A\int d^2\mathbf{q}\{K_c q^4+\sigma q^2+V''\}\tfrac{1}{2}|h_q|^2 , \quad (3)$$

where $q=\sqrt{q_{x_1}^2+q_{x_2}^2}$ denotes the wave vector. The thermal average of the square of the Fourier amplitudes for each wave vector can be calculated from Eq. (3). Applying the equipartition theorem the static power spectrum of the mean square amplitudes is given by

$$\langle h_q^2\rangle=\frac{k_B T}{A\{K_c q^4+\sigma q^2+V''\}} . \quad (4)$$

The power spectrum depends on the parameters K_c,σ, and V'' and exhibits distinctive regimes, where each of the parameters dominates depending on the wave vector q. Note that the area A over which the Fourier transformation is carried out can be arbitrarily chosen and acts as a normalization factor.

vdW and steric interaction

In the absence of electrostatic surface charges the only long-ranged direct interaction is the van der Waals interaction. Taking into account the finite thickness d of the membrane and assuming that the substrate extends

infinitely in one direction, the vdW interaction is given by

$$V_{\mathrm{vdW}}(s)=-\frac{A_H}{12\pi}\left[\frac{1}{s^2}-\frac{1}{(s+d)^2}\right], \tag{5}$$

where A_H is the Hamaker constant. For biological material immersed in water A_H is of the order (1–4)kT. At large distances ($s>\approx 5$ nm) retardation decreases the nonzero-frequency part of the Hamaker constant. Therefore a lower limit for very large separations is given by $A_{H(v=0)}\approx\frac{3}{4}kT$ in the case of dielectrics in aqueous solution [15]. In the presence of ions the van der Waals interaction is furthermore screened as described by Mahanty and Ninham [16]. The effective Hamaker constant is

$$A_H^{\mathrm{eff}}(0)=A_H(0)(2\kappa_D s)\exp(-2\kappa_D s)$$

for $\kappa_D s>1$ with κ_D^{-1} being the Debye screening length.

The second interaction to be considered is the steric interaction of undulating membranes. It arises from the thermally excited out-of-plane fluctuations that repel the membrane from the hard wall. In order to derive the steric interaction it is helpful to consider the height-autocorrelation function of the membrane $C(\mathbf{x})=\langle h(\mathbf{x})h(\mathbf{0})\rangle$. The autocorrelation function can be directly obtained by Fourier transformation of the frequency spectrum of the thermal surface roughness already described by Eq. (4) (the Wiener-Khinchin theorem). In a simplified form $C(\mathbf{x})$ is approximated by its exponential asymptotic behavior:

$$C(\mathbf{x})=\langle h(\mathbf{x})h(\mathbf{0})\rangle=\xi_\perp^2 e^{-x/\xi_\parallel}. \tag{6}$$

Two lengths are introduced: the lateral correlation length $\xi_\parallel$ and the vertical roughness amplitude $\xi_\perp$. Both length scales can be expressed in terms of the parameters V'',σ, and K_c. Approximate expressions can be given [17] depending on whether the membrane tension is large or small compared to the bending modulus, with a crossover tension given by $\sigma^*=\sqrt{4K_cV''}$. It follows from Eq. (4) that

$$\xi_\perp^2=\begin{cases}\dfrac{kT}{8\sqrt{K_cV''}} & \text{for } \sigma<\sigma^* \quad (7a)\\[2ex] \dfrac{kT}{2\pi\sigma}\ln(2\sigma/\sigma^*) & \text{for } \sigma>\sigma^*, \quad (7b)\end{cases}$$

and

$$\xi_\parallel\approx\begin{cases}(4K_c/V'')^{1/4} & \text{for } \sigma<\sigma^* \quad (8a)\\ (\sigma/V'')^{1/2} & \text{for } \sigma>\sigma^*. \quad (8b)\end{cases}$$

For small tensions $\sigma<\sigma^*$ the characteristic length scales are dominated by the bending rigidity while for large tensions $\sigma>\sigma^*$ the lengths are tension dominated. Equations (7) and (8) can be combined to obtain the interdependence of $\xi_\parallel$ and $\xi_\perp$:

$$\xi_\perp^2\approx\begin{cases}\dfrac{kT}{16K_c}\xi_\parallel^2 & \text{for } \sigma<\sigma \quad (9a)\\[2ex] \dfrac{kT}{4\pi\sigma}\ln(\sigma\xi_\parallel/K_c) & \text{for } \sigma>\sigma^*. \quad (9b)\end{cases}$$

In the zero-tension limit, Eq. (9a) states a universal scaling law $\xi_\perp\sim\xi_\parallel^\zeta$ with roughness exponent $\zeta=1$ [8].

We will now consider the interaction between two flat membranes that are not trapped in a potential, but located close to each other. From the description above, an undulating surface can be pictured as a surface with random humps of typical height $\xi_\perp$ extending over an area $A_{\mathrm{sq}}\approx\xi_\parallel^2$. In the original Helfrich work these humps were interpreted in terms of independent particles that exert an ideal gas pressure, $P_{\mathrm{steric}}\approx kT/\xi_\parallel^2$ [1,19]. The distance dependence of this steric interaction is derived by substitution of $\xi_\parallel$ through Eq. (9a) and by assuming a constant ratio $c_\perp$ of the roughness $\xi_\perp$ to the separation distance $\xi_\perp=c_\perp\langle s\rangle$. The steric interaction energy per area is given by

$$V_{\mathrm{steric}}=c_{\mathrm{fl}}\frac{(kT)^2}{K_c\langle s\rangle^2}. \tag{10}$$

Here c_{fl} denotes a dimensionless prefactor that determines the strength of the fluctuation-induced interaction. This prefactor was estimated by Helfrich as $c_{\mathrm{fl}}=3\pi^2/128=0.231$ for two interacting membranes with bending modulus K_c [1,9]. The fluctuation-induced interaction is recovered by functional renormalization of the hard-wall interaction and leads to the same inverse square dependence on the separation distance. Monte Carlo simulations of the steric interaction yield slightly smaller prefactors. Lipowsky and Zielinska found $c_{\mathrm{fl}}=0.116$ [20], Janke and Kleinert $c_{\mathrm{fl}}=0.074$ [21], and Gompper and Kroll $c_{\mathrm{fl}}=0.0798$ [22]. In an analytical study Podgornik and Parsegian find $c_{\mathrm{fl}}=0.043$ [23].

In the presence of membrane tension the roughness behavior $\xi_\perp(s)$ changes from a linear to a logarithmic dependence on the membrane separation. A crossover length scale for this case is given by $l_\sigma=\sqrt{kT/2\pi\sigma}$ [17,25].

$$\xi_\perp=\begin{cases}c_\perp\langle s\rangle & \text{for } \xi_\perp<l_\sigma \quad (11a)\\ l_\sigma\left[\dfrac{\langle s\rangle}{2l_\sigma}+\frac{1}{8}\ln(\langle s\rangle/l_\sigma)\right]^{1/2} & \text{for } \xi_\perp>l_\sigma. \quad (11b)\end{cases}$$

The steric free energy for finite tension is again obtained from the ansatz $P_{\mathrm{steric}}\approx kT/\xi_\parallel^2$. Following the same steps as before, applying Eqs. (9b) and (11b) leads to [17,25]

$$V_{\mathrm{steric}}^\sigma=b_{\mathrm{fl}}\frac{k_BT\sigma}{K_c}e^{-s/l_\sigma}(l_\sigma/s)^{1/4} \quad \text{for } \xi_\perp>l_\sigma. \tag{12}$$

The interaction energy decays exponentially with the mean separation distance $\langle s\rangle$. It can be shown that the

prefactor b_{fl} is related to the prefactor in the case without tension through $b_{fl}=4\pi c_{fl}c_{\perp}^2$ [17,25]. For a single membrane interacting with a hard wall by a short-ranged attractive interaction the ratio $c_{fl}\approx 1$ was found [24,25]. Furthermore, the effective bending modulus of two interfaces with different bending modulus K_1 and K_2 is given by $K_{eff}=2K_1K_2/(K_1+K_2)$. Therefore, in the case of a single membrane interacting with a rigid wall ($K_1=K_c$ and $K_2=\infty$), the effective bending modulus is twice the modulus of one membrane $K_{eff}=2K_c$. The strength of the steric interaction of one membrane under tension with a hard wall is hence well approximated by $b_{fl}=2\pi c_{fl}c_{\perp}^2\approx 0.085$. Qualitatively any tension drastically diminishes both the strength and the range of the undulation forces. In fact any finite tension will change the unbinding behavior of membranes. Exact renormalization group theory predicts a continuous unbinding transition for the zero-tension limit [18]. In contrast, a first order unbinding transition is expected for finite tension [26].

The total interaction potential of a membrane under tension and a solid flat substrate can be approximated by simple superposition of the vdW interaction and the steric interaction. The superposition as opposed to a rigorous renormalization approach is valid if the fluctuations are weak, which for membranes under tension is always the case [26]. For the experimental situation as described later on it is also of interest to consider the gravitational force, as vesicles can exhibit a density difference with respect to the buffer solution. The free energy is given by a linear potential provided the shape of the vesicle does not change with the mean separation distance, $V_{grav}=-g\Delta\rho\langle s\rangle V_V/A_C$. Here V_V/A_C denotes the ratio of volume and contact area. The total interaction energy now reads

$$V_{total}\approx V_{steric}+V_{vdW}+V_{grav}\ . \tag{13}$$

The three interaction potentials and their superposition are shown in Fig. 2 for a particular set of parameters ($\sigma=1.7\times10^{-5}$ J/m^2, $A_H=2.6\times10^{-21}$ J/m^2, $c=10^{-4}$ molar, $\Delta\rho=0.007$ g/cm^3, $b_{fl}=0.085$, $D_M=20$ μm, $D_A=10$ μm). In the range of these values the superposition yields a minimum at a remarkably large separation distance. The position of the minimum decreases with increasing tension, while the depth and curvature of the minimum increase. Note that the contribution of the gravitation is weak and does not strongly affect the position of the minimum. A membrane in this kind of bound state will exhibit a fluctuation spectrum as given by Eq. (4). The parameter V'' corresponds to the curvature of the minimum of the interaction energy. From Fig. 2 it can also be seen that the harmonic approximation for the interaction V_{total} made earlier to obtain Eq. (4) from Eq. (2) is justified. The depth of the minimum shown in Fig. 2 can be considered to first approximation as the adhesion energy per area of the membrane.

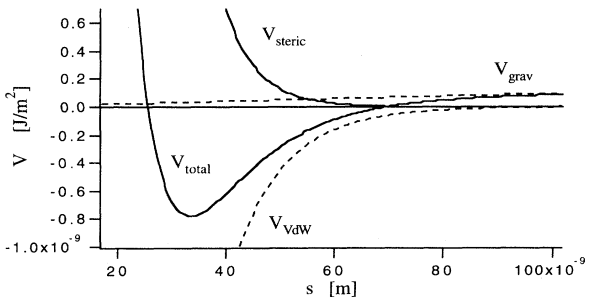

FIG. 2. The total interaction potential calculated by superposition of van der Waals interaction (dashed line), steric interaction (full line), and gravitation (dashed line). The superposition (full line) exhibits a minimum that moves towards smaller values as the tension increases. ($\sigma=1.7\times10^{-5}$ J/m^2, $K_c=35kT$, $b_{fl}=0.085$, $A_H=2.6\times10^{-21}$ J, $c=10^{-4}$ molar, $D_M=20$ μm, $D_A=10$ μm, $\Delta\rho=0.007$ g/cm^3).

Adhering vesicles

In the case of vesicles adhering to a substrate only the adjacent part of the vesicle is subject to the interaction potential as described above. The overall shape of the vesicle at an attractive wall is determined by the bending modulus of the membrane as well as the constraints of constant surface area and constant enclosed volume. The vesicle gains adhesion energy by increasing its contact area but pays for the shape change through bending energy. The equilibrium shape of adhering vesicles has been studied theoretically in detail [14]. It can be shown that a general boundary condition holds for the shapes of minimal free energy. Due to the elastic bending energy the membrane will not meet the solid surface at a sharp contact angle, but rather exhibits a contact curvature described by the radius of curvature R_c. For radii small compared to the dimensions of the vesicle the following equation holds:

$$R_c=\sqrt{K_c/2W_A}\ . \tag{14}$$

However, on a larger scale an effective contact angle ϑ_{eff} defined by the tangent of the contact contour can be defined for which the well-known Young-Dupre equation holds:

$$W_A=\sigma(1-\cos\vartheta_{eff})\ , \tag{15}$$

where σ denotes the membranes tension and W_A the adhesion energy per area.

As shown by Eq. (15), adhesion induces tension in the membrane. The elastic response of the free part of the vesicle membrane to tension is twofold. First, tension will reduce the excess area consumed by the thermal fluctuations and, secondly, high tension will eventually stretch the actual membrane area. The apparent dilation $\alpha=(A-A_0)/A_0$, i.e., the relative change in area projected at the equilibrium contour of the vesicle, can be written as follows [10,27,28]:

$$\alpha=\frac{A-A_0}{A_0}=\frac{kT}{8\pi K_c}\ln\frac{\sigma a^2}{K_c\pi^2}+\frac{1}{K_a}\sigma\ . \tag{16}$$

The first term on the right side of Eq. (16) describes the

entropic excess area that is taken up by the undulations and that is pulled out by tension. The length a is a microscopic length scale that determines the short-wavelength cutoff of the undulations. The second term denotes the elastic stretching of the lipid bilayer with the elastic area dilation modulus K_a. Equation (16) can also be used to determine the "effective tension," if the area dilation α is fixed by boundary conditions. A vesicle that is only slightly deflated, such that the boundary conditions of fixed volume and fixed surface area restrict the undulations, can be described as being subject to an effective tension according to Eq. (16).

It must be noted that the effective tension has to be worked out in a self-consistent way, since the excess area depends on the adhesion energy and the adhesion energy depends on the tension. However, a rigorous theory of the equilibrium shape of adhering vesicles including fluctuations does not exist yet.

EXPERIMENTAL

Microscope setup and image processing

Adhering vesicles were observed with RICM combined with phase contrast microscopy. Reflection interference allows visualization and measurement of the adjacent contact contour of the vesicle. Phase contrast microscopy images the lateral circumference of the vesicle. The two microscopic techniques can be applied simultaneously choosing alternatingly epi- or dia-illumination, respectively.

We used an inverted Zeiss Axiomat microscope equipped with a Zeiss Neofluar 63/1.25 Antiflex objective. Epi-illumination was provided by a 100 W high pressure mercury lamp. The green 546.1 nm Hg line was selected by a bandpass filter ($dv=5$ nm, 85%) for reflection interference. The illumination aperture was adjusted to its smallest value of $INA \approx 0.48$. Phase contrast microscopy was performed with conventional Köhler illumination. Since the Antiflex objective had no built-in phase ring a phase ring was placed in an artificial back focal plane.

A detailed quantitative analysis of the RICM images of membranes has been given recently by us [13]. The surface profile can be obtained from the measured intensities. A schematic view of the technique is given in Fig. 3. The image is formed by interference of the light reflected from the membrane and from the substrate. The intensity of the interference pattern can be written in the form

$$I(s(x))=I_1+I_2+2\sqrt{I_1 I_2}\cos[2ks(x)-\delta_1+\delta_2] , \quad (17)$$

where the term in square brackets denotes the phase difference due to the difference in the optical path $2ks=4\pi ns/\lambda$. The intensities and initial phases of the beams I_1,δ_1 and I_2,δ_2 can be calculated using Fresnel equation for layered dielectrics [29]. As an example, Fig. 3(b) shows the interference function Eq. (17) with and without a magnesium fluoride layer coating the glass surface. It is apparent that the interference function can be shifted by an appropriate substrate structure [13]. We have chosen the thickness of the magnesium fluoride layer in such a way that the intensity increases monotonically with the membrane-substrate separation distance in the range $0<s<100$ nm. The distance $s(x)$ can be calculated from the measured intensities $I(x)$; we obtain from Eq. (17)

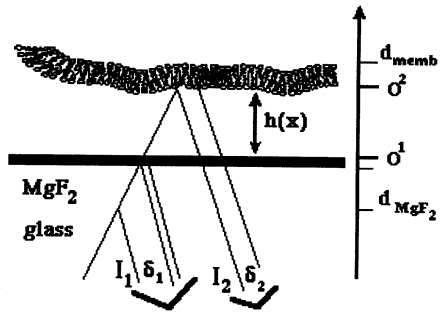

(a)

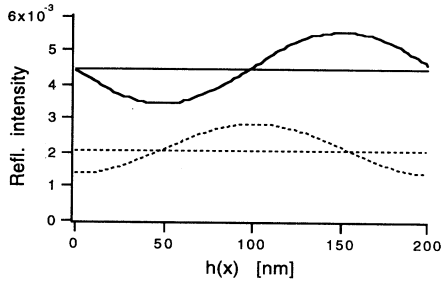

(b)

FIG. 3. Schematic view of image formation in reflection interference contrast microscopy. (a) Formation of image by interference of light reflected from the substrate (I_1) and from the membrane (I_2). (b) Relative intensity reflected from a phospholipid membrane versus distance above the substrate for glass (solid line) and glass coated with 60 nm MgF_2 (dashed line).

$$s(x)=\frac{\lambda}{4\pi n}\left[\arccos\left[\frac{2I(x)-(I_{\max}+I_{\min})}{I_{\max}-I_{\min}}\right]+\delta_1-\delta_2\right] . \quad (18)$$

The values $I_{\max}$ and $I_{\min}$ may be calculated or taken from the observed interference picture. Equation (18) provides a gauge function that, once established for a given substrate-membrane system, related the intensities to heights.

Data processing

Images were recorded by a charge-coupled device (CCD) camera (HR480, Aqua TV, Germany) and a Panasonic video recorder with standard video rating (25 Hz). Images were read into a Macintosh Quadra using the Pixelpipeline frame grabber (Perceptics Co.). Regions of 256×256 pixels were selected and a sequence of 64 frames stored in real time.

Height images as obtained in the previous section are

digitized and read into the computer via frame grabber card. Each two-dimensional picture consists of 480×630 picture elements (pixels) indexed by (m,n) and each having an integer $H(m,n)$ proportional to the separation distance attributed. A pixel corresponds to a quadratic field with length $dx=dy=94$ nm in real space. Movies of flickering adhering vesicles are analyzed by choosing a region of $N\times N$ pixels in the adhering part of the vesicle and taking a sequence of height images $H(m,n,t_j)$ at times t_j $(j=1,\ldots,M)$. The discrete Fourier transform of the height values in the selected $N\times N$ field is determined according to Eq. (1):

$$H(m,n,t_j)=\sum_{k=0}^{N-1}\sum_{l=0}^{N-1}\tilde{H}(k,l,t_j)e^{i2\pi mk/N}e^{i2\pi nl/N},$$

$$\tilde{H}(k,l,t_j)=\frac{1}{N^2}\sum_{m=0}^{N-1}\sum_{n=0}^{N-1}H(m,n,t_j)e^{-i2\pi mk/N}e^{-i2\pi nl/N}. \tag{19}$$

Recalling that the selected area has the dimensions $A=L^2=(Ndx)^2$ the wave vector is given by $q=2\pi/L(k,l)$ with $k,l=0,\ldots,N-1$. The Fourier transforms $\tilde{H}(k,l)$ are complex numbers with $H^*(k,l)=\tilde{H}(-k,-l)$.

The squares of the absolute values of the Fourier components are averaged over time according to

$$\langle\tilde{H}^2(k,l)\rangle=\frac{1}{M}\sum_{j=1}^{M}\tilde{H}^2(k,l,t_j). \tag{20}$$

With our choice of normalization, Parseval's theorem demands

$$\sum_{k=0}^{N-1}\sum_{l=0}^{N-1}\tilde{H}^2(k,l,t_j)=\frac{1}{N^2}\sum_{m=0}^{N-1}\sum_{n=0}^{N-1}H^2(m,n,t_j) \tag{21}$$

which proves useful as a test for the numerically determined mean square amplitudes of the Fourier transform compared to the original height data.

Sample preparation

Giant vesicles were prepared from a chloroform-methanol (2:1) solution of stearoyl-oleoyl-phosphatidylcholine (SOPC) (Avanti Polar Lipids, Alabaster) at a concentration of 10 mg/ml. 40 ml of the solution was dried on a Teflon disk and desiccated under vacuum for 2 h. 100 mM sucrose solution was then added to the Teflon disk in a glass beaker and left for 24 h at 40 °C. In this time the lipid detaches from the bottom and forms closed vesicles. Alternatively, the electrical swelling method that generally yields larger vesicles was applied [30]. A stock solution of lipid was dried onto indium tin oxide (ITO) glass cover slips (Balzers, Lichtenstein). After desiccation the cover slips were placed in a sucrose solution and an ac field of 18 V/cm, 10 Hz was applied for 1 h.

Glass cover slips ($20\times20\times0.17$ mm^3) were covered with a thin film of MgF_2 by MgF_2-vapor deposition in vacuum. The deposition was carried out at a pressure of 10^{-6} atm with a deposition rate of 1 nm/s and a substratum temperature of 380 °C. The film thickness was measured by a quartz thickness monitor. The refractive index and thickness of the MgF_2 film were cross-checked by quantitative evaluation of RICM images as described previously [13]. The MgF_2 covered coverslip was then mounted onto the measuring chamber consisting of a thin Teflon frame embedded in a temperature-controlled copper block.

The MgF_2 surface was covered with bovine serum albumin (BSA) to prevent strong adhesion. A solution of 5 μg/ml BSA was adsorbed onto the MgF_2 substrate for 15 min and then rinses afterwards. The MgF_2 surface remains covered with a thin layer of BSA after this treatment (20 Å). A suspension of vesicles was then added onto the substrate and the adhesion observed with RICM.

RESULTS

Equilibrium contact shape

Figure 4(a) shows a micrograph of a SOPC vesicle that weakly adheres to a BSA covered MgF_2 surface. Only the substrate adjacent part is imaged, showing clearly the adhering flattened region surrounded by fringes that cor-

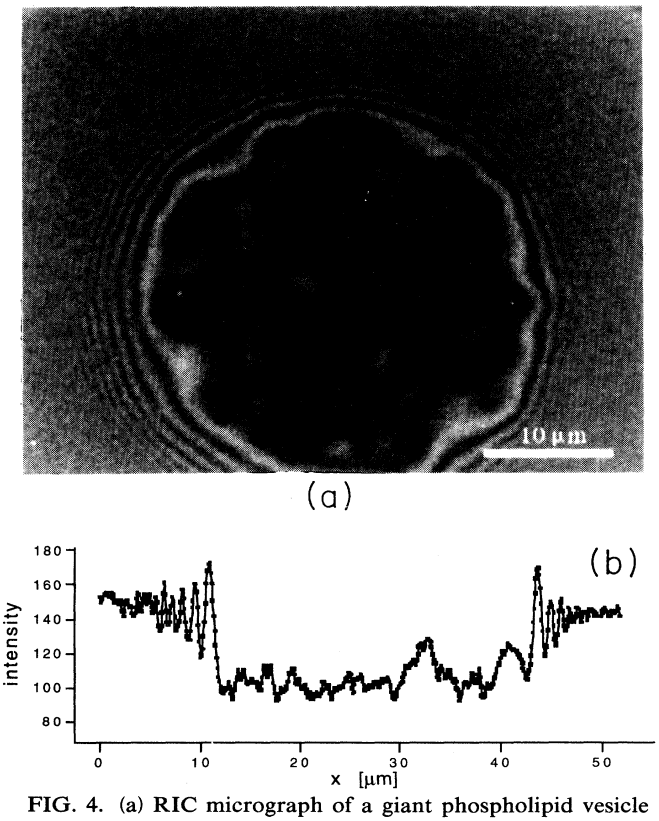

FIG. 4. (a) RIC micrograph of a giant phospholipid vesicle above a BSA coated MgF_2 substrate. The fringes at the edge of the round contact area arise from the up-bending profile. (b) Intensity scan through center of contact area. The momentary intensity of one frame reflects the distorted contour of the membrane by thermal fluctuations.

respond to the edge contour. The outer contour with diameter D_M is not shown but can be measured by observing the vesicle under phase contrast microscopy. A transient intensity profile through the center of Fig. 4(a) is given in Fig. 4(b). The equilibrium contour of the vesicle can be determined as follows. First from the middle part of Fig. 4(b), where the intensities belong to the zero order fringe, the substrate vesicle distance $s(x)$ can be directly calculated by applying Eq. (18). The resulting height profiles are then averaged over 64 frames. Figure 5(a) shows the profile for the region around one edge. The adhering part appears fairly flat since the undulations are averaged out. On the right hand side of the plot the height function exhibits extrema corresponding to higher order fringes. These extrema do not reflect the actual profile; rather they can be used to obtain additional data points [⊞ in Fig. 5(b)], with the assumption that the surface bends monotonically away from the surface. The extrema correspond to heights

$$h_j = \frac{j\lambda}{4n} + \arccos(\delta_1 - \delta_2) \tag{22}$$

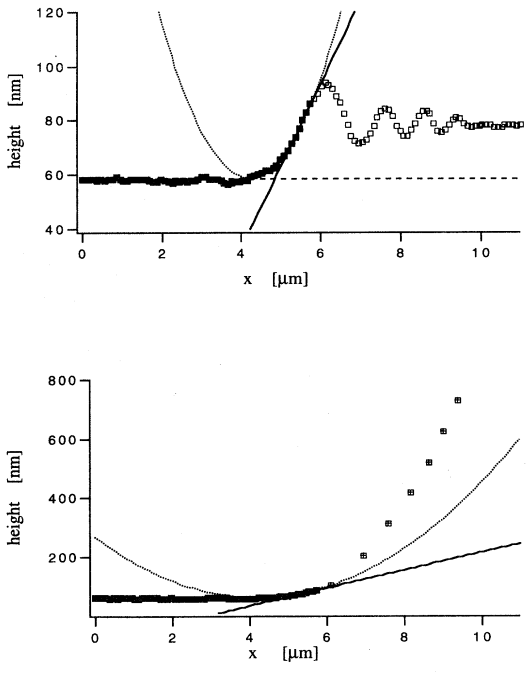

FIG. 5. (a) Edge contour of a vesicle obtained by converting the intensity profiles into heights [Eq. (18)] and taking the average over 64 height profiles. The dark rectangular data points correspond to the regime $s < 100$ nm; the open data points correspond to higher order fringes and are not further considered. A contact angle and a circle are tentatively fitted into the contact contour. Note that the scales are distorted. The measured contact angle is extremely flat ($\vartheta \approx 1°$). (b) Same contour as (a) shown on a larger scale. The extrema of the higher order fringes in (a) are represented here by single data points separated by 104 nm in the vertical direction.

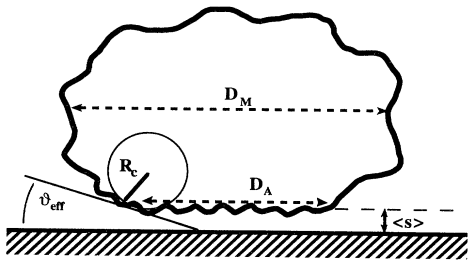

FIG. 6. Schematic view of a vesicle above a substrate. D_M is the vesicle diameter, D_A is the diameter of the contact region, ϑ_{eff} is the effective contact angle in the azimuthal, $1/R_c$ gives the curvature at the contact edge, and $\langle s \rangle$ is the mean height of the vesicle above the substrate.

with j an integral number and n, δ_1, and δ_2 as defined in Eq. (17). The result for the contour in Fig. 5(a) is depicted in Fig. 5(b). Note that the scales are different in x and s. Therefore the real shape of the measured contour is extremely flat.

Figure 5(a) shows how the contact angle is determined by fitting a straight line to the edge contour. The contact angle in this region close to the surface is of the order of 1°. In Fig. 5(b) it can be seen that the contour bends away very strongly and that measuring the contact angle on a larger scale would lead to considerably larger contact angles.

Figures 5(a) and 5(b) also depict a best fit of a circle into the bending edge [dotted line in Fig. 5(a); note again the distortion due to different scales]. Fitting the radius of curvature is, however, often obscured by fluctuations in the membrane profile that remain even after averaging. Also we obtain radii of curvature R_c of the same magnitude as the diameter of the vesicle, implying that Eq. (14) cannot be applied.

In summary, the averaged micrographs yield the parameters depicted schematically in Fig. 6: the diameter D_A of the adhering area, the diameter D_M of the vesicle in the midplane, the mean separation distance $\langle s \rangle$, and the effective contact angle ϑ_{eff}. The measured values for several vesicles are listed in Table I.

TABLE I. Values of the parameters defined in Fig. 6 for nine different vesicles.

D_M (μm)	M_A (μm)	ϑ_{eff} (deg)	$\langle s \rangle$ (nm)	σ (10^{-6}J/m^2)	V'' (10^6 J/m^4)	$\xi_\perp$ (nm)	$\xi_\parallel$ (nm)
69	60		40.8	41.9	15.0	6.2	746
52	17	1.4	38.4	87.3	58.3	4.3	758
58	10	2.1	36.7	51.1	499	3.7	115
55	18	2.1	39.5	4.2	4.0	15.1	723
88	45	0.8	48.7	8.1	6.8	11.0	792
62	27	1.1	39.6	14.5	17.6	8.8	700
53	15	0.7	40.8	17.3	13.1	8.8	870
83	64	2.1	31.1	27.3	16.1	8.8	733
91	31	0.9	36.0	15.9	16.8	9.7	740

Static fluctuation spectrum

In the flat part of the adhering vesicle the membrane fluctuations can be treated as a superposition of plane waves. This approximation is valid for wavelengths shorter than the diameter of the contact area. We took sequences of undulation profiles and analyzed a square region $A=L\times L$ of the adhering part. The measured intensities were transformed into heights $s(x_1,x_2)$ and a numerical Fourier transformation was carried out as described above [Eqs. (19) and (20)]. Figure 7(a) shows the spectrum of the fluctuations. The mean square amplitudes $\langle h^2(q_{x_1},q_{x_2})\rangle$ of the two-dimensional field are plotted as a function of $q=\sqrt{q_{x_1}^2+q_{x_2}^2}$. (Hence multiple data points are obtained for most q values.) The data can be fitted by Eq. (4) with V'' and σ being adjustable parameters. The values for the membrane tension σ and the second derivative of the interaction potential are listed in Table I.

The fit shown in Fig. 7(a) deviates for q values larger than $2\ \mu m^{-1}$. In this high wave vector regime the experimental amplitudes are too small for two reasons. First, the relaxation times of the modes decrease strongly with increasing q and the short-wavelength fluctuations are averaged out owing to the finite integration time of the CCD camera [8]. Secondly, the resolution of the microscope is limited, which means that the imaged amplitude of a sinusoidal intensity profile is somewhat smaller than the true amplitude as the optical resolution limit is reached. A correction of the amplitudes of the experimental power spectrum can be carried out to yield better agreement, if the relaxation times of the modes and the optical transfer function are known. In this case the bending modulus K_c could be measured accurately as well. We will address the dynamics of the fluctuations and measurement of the relaxation times in a forthcoming article. In this article we have taken the bending modulus $K_c=35kT$ for SOPC as measured by other techniques [7,11].

It is worthwhile to look at the fluctuations also in terms of the correlation function. The autocorrelation function can be obtained simply by Fourier transformation of $\langle h_q^2\rangle$. The autocorrelation function calculated by Fourier transformation is identical to the autocorrelation obtained by directly correlating the undulation profile $h(x_1,x_2)$, as it should be. Figure 7(b) shows the autocorrelation function as obtained from Fig. 7(a). The autocorrelation function exhibits a steady decay without oscillations into negative values. An exponential function

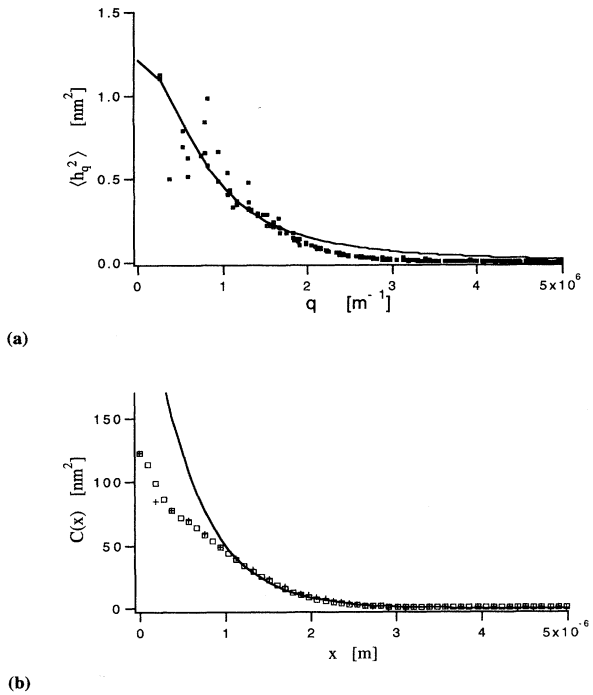

FIG. 7. (a) The mean square amplitudes of the Fourier components plotted as a function of the wave vector q. The power spectrum is fitted according to Eq. (4), yielding the second derivative of the interaction potential, and the membrane tension is obtained. The discrepancy between measured and calculated data at large wave vectors is due to limited spatial and time resolution. (b) Autocorrelation function obtained from (a) by Fourier transformation. The vertical roughness is obtained from $C(0)$ and the parallel correlation length is obtained from the single exponential fit to the tail region of the correlation function.

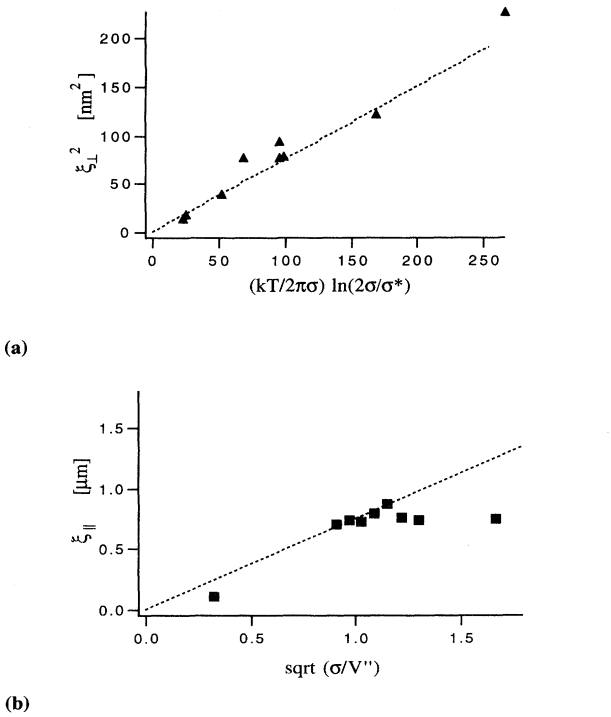

FIG. 8. (a) Vertical roughness obtained from the autocorrelation $C(x)$ as a function of the parameters obtained from best fits of the power spectrum [Eq. (7)]. (b) Lateral correlation length obtained from the autocorrelation as a function of the parameters obtained from best fits of the powerspectrum [Eq. (8)].

is fitted to the asymptotic decay that yields the lateral correlation length $\xi_\parallel$. The vertical roughness is defined by the value $C(0)=\xi_\perp^2$. Both values are listed in Table I.

As discussed in the theoretical section there are asymptotic equations which allow one to express $\xi_\perp$ and $\xi_\parallel$ in terms of the parameters V'', σ, and K_c. For tensions larger than the crossover tension $\sigma^*=\sqrt{4K_cV''}$ Eqs. (7b) and (8b) apply. As can be seen from Table I, the measured values of σ are in fact about 20 times larger than the cross over tension. Figures 8(a) and 8(b) demonstrate the validity of Eqs. (7b) and (8b). The data in Fig. 8(b) deviate for higher tension, which might possibly indicate that we do not obtain the true lateral correlation length for high tension by an exponential fit. In general Fig. 8 should be understood as a test of self-consistency of fit parameters obtained from data analysis in Fourier and real space respectively.

Tension-induced adhesion

A key relation in the theory of steric interaction is the behavior of the vertical roughness as a function of separation distance and tension. In Fig. 9 we plotted the experimental vertical roughness versus the logarithmic expression Eq. (11b) of the separation distance in units of the crossover length $l_\sigma=\sqrt{kT/2\pi\sigma}$. The mean separation distances and corresponding tensions have been taken as determined from the static fluctuation spectrum of the vesicles. The dashed line indicates the theoretical prediction. The functional dependence as given by Eq. (11) is roughly obeyed. However, the data fall systematically below the theoretical values. A possible explanation is that the constrains of finite camera integration time and finite optical resolution average out the undulations of high spatial frequency and therefore result in the measurement of an altogether smaller vertical roughness.

We may now compare the experimental data with the theory of undulating membranes under tension. Figure 10 depicts the mean separation distance $\langle s(\sigma)\rangle$ as a function of membrane tension. The separation distance decreases slightly with higher tension as indicated by the straight dashed line. The scatter of the data is considerable though. In fact, while the relative displacement can be measured very accurately within 1 nm, the measurement of the absolute separation distance depends on the precise knowledge of the thickness and refractive index of the deposited MgF_2 layer and is therefore less accurate.

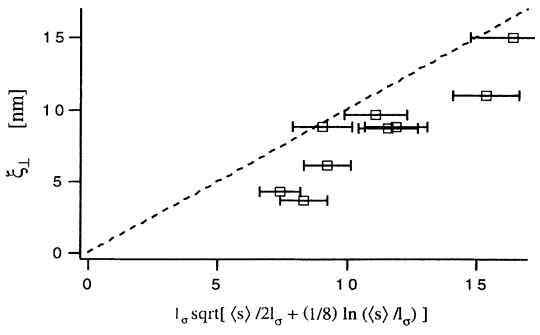

FIG. 9. Vertical roughness plotted versus the separation distance $s(x)$. The roughness behavior follows the relation predicted by Monte Carlo studies [Eq. (11), dashed line with slope 1], but shows systematic deviations towards smaller roughness due to the limited spatial and time resolution of the camera.

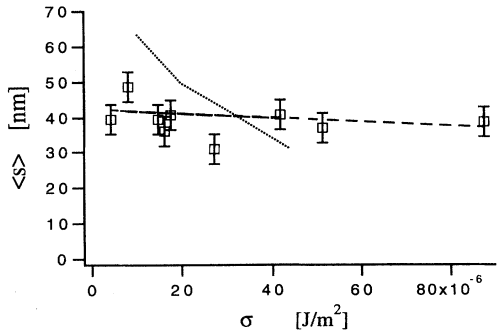

FIG. 10. The membrane separation distance as a function of the membrane tension. The dotted line depicts the theoretical values calculated by superimposing vdW interaction, steric interaction, and gravitation (compare also Fig. 2). The data, however, follow a weaker dependence of the separation distance with tension as indicated by the dashed line.

However, it is worthwhile comparing the data with the theoretical values expected from the superposition of the steric interaction and vdW interaction. We assume the following material constants. The Hamaker constant for lipid interacting with MgF_2 in water can be estimated using the Lifschitz approximation [15]. Taking the values $n_{\text{lipid}}=1.486$, $\varepsilon_{\text{lipid}}(0)=2.1$ for the membrane and $n_{MgF_2}=1.386$, $\varepsilon_{MgF_2}(0)=7$ for magnesium fluoride, the zero-frequency part of the Hamaker constant is calculated to be $A_H(\omega=0)=2.6\times10^{-21}$ J and $A_H(\omega>0)=2.2\times10^{-21}$ J. We furthermore assume an ion concentration of 10^{-3} molar, taken from the small but finite solubility of MgF_2. The bending modulus was measured independently, $K_c=35kT$, as mentioned above. In order to take the gravitational field into account, we assume an average vesicle of diameter $D_M=40$ μm and a contact area of diameter $D_A=20$ μm. The density difference of a 100 mM sucrose solution with respect to a 100 mM inositol solution is given by $\Delta\rho=0.007$ g/cm^3. The prefactor for the steric interaction, Eq. (12), was taken as $b_{\text{fl}}=0.085$, as derived in the theoretical section. Eventually we obtain from the minimum of the total interaction potential (compare Fig. 2) the dashed line indicated in Fig. 10. Clearly the theoretical calculation predicts a stronger dependence of the separation distance on the membrane tension. However, the calculation also shows that the superposition model predicts mean separation distances in the correct order of magnitude as measured. It must be noted that the theory holds no adjustable parameter and no additional assumptions are needed.

Adhesion energy

The adhesion energy $W_A(\sigma)$ can be determined from the equilibrium contact angle using the Young-Dupre

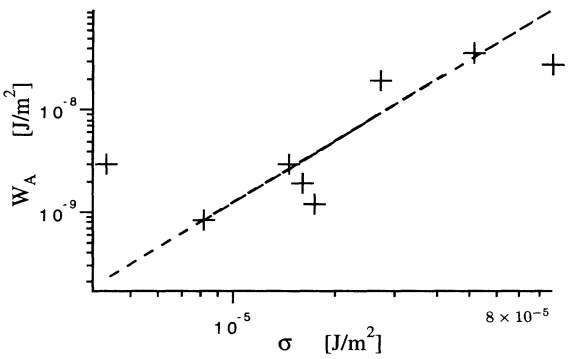

FIG. 11. The adhesion energy calculated from the measured contact angles [Eq. (15)] as a function of the membrane tension depicted in a double logarithmic plot. The dashed line indicates a slope 2.

equation, Eq. (15). In Fig. 11 we show the adhesion energy as obtained from the contact angle and the measured membrane tension σ. The plot is given on a double logarithmic scale and indicates a quadratic dependence of the adhesion energy as a function of tension (the straight line has slope 2). The strength of the adhesion energy is found to be 10^{-9}–10^{-8} J/m^2 and therefore larger than the depth of the minimum obtained from the superposition of vdW and steric interaction alone. Hence it must be assumed that gravity determines the measured adhesion energy. However, the discrepancy remains unresolved so far.

Our results disagree with previous measurements of vesicle-vesicle adhesion where constant contact angle of the order 35° were measured and therefore a linear dependence of adhesion energy and tension established [10,12]. However, it must be noticed that these experiments differ in at least two important facts. First of all the strength of the vdW interaction varies due to different buffer conditions as well as due to the fact that in the latter case two vesicles rather than a vesicle and a wall interact. The van der Waals interaction for two membranes of thickness d scales at large distances $V_{\mathrm{vdW}} \sim 6d^2/s^4$ ($s \gg d$), in contrast to the case of a membrane interacting with a solid surface, where $V_{\mathrm{vdW}} \sim 2d/s^3$ ($s \gg d$) is found. Secondly, gravity has in our experiments an effect on the membrane tension as well as the overall shape of the vesicle. In fact, the shape of the vesicle and also the measured contact angles can be dependent on gravitational effects.

CONCLUSION

We have shown that reflection interference contrast microscopy is a powerful technique for quantitative studies of vesicle adhesion. The contact contour of several SOPC vesicles adhering to BSA coated MgF_2 substrates was determined. In the flat contact zone of the membrane an analysis of the static out-of-plane fluctuations yields the membrane tension and the second derivative of the interaction potential. The autocorrelation function of the undulations yielded the vertical roughness and the lateral correlation length. Altogether six parameters can be extracted independently, i.e., the membrane tension and the harmonic approximation of the interaction potential (or alternatively the lateral correlation length $\xi_\parallel$ and the vertical roughness amplitude $\xi_\perp$), as well as the membrane-substrate separation distance, the contact angle, the diameter of the vesicle, and the diameter of the adhesion area.

Of these parameters the relative displacement and therefore the static fluctuation spectra can be measured very precisely, whereas the absolute separation distance can only be measured approximately. The measured roughness versus separation distance indicates clearly a tension-dominated fluctuation behavior, which is in good agreement with the predicted logarithmic dependence on the separation distance. The quantitative comparison of the dependence of the membrane-substrate separation distance on the membrane tension with the superposition model yields the correct order of magnitude for the separation distances but a weaker dependence on the tension. Furthermore, the adhesion energies were found to depend quadratically on the membrane tension.

Conceptually the following problem remains unsolved. So far we cannot relate the equilibrium shape of the adhering vesicle to the static fluctuation spectrum. The measurable membrane tension is expected to depend on the shape of the vesicle, i.e., the volume and the surface area. On the other hand the membrane tension determines the adhesion energy through the steric interaction and the adhesion energy in turn affects the equilibrium contour of the vesicle. In a self-consistent description the effective membrane tension will be the key variable controlling the steric interaction and the equilibrium shape. We hope that this article will encourage future theoretical work.

ACKNOWLEDGMENTS

This project was funded by the DFG through the SFB 266. T.F. is grateful for support from the Alexander von Humboldt Stiftung. We thank E. Evans, G. Gompper, W. Helfrich, J. Israelachvili, M. Kraus, R. Lipowsky, R. Netz, and U. Seifert for many helpful discussions. We are particularly grateful to M. Kraus, R. Lipowsky, and U. Seifert for sharing their unpublished results with us.

[1] W. Helfrich, Z. Naturforsch. Teil A **33**, 305 (1978).

[2] D. R. Nelson, in *Proceedings of the Fifth Jerusalem Winter School,* edited by D. R. Nelson, T. Piran, and S. S. Weinberg (World Scientific, Singapore, 1989); R. Lipowsky, Nature **349**, 471 (1991).

[3] E. Sackmann, in *Structure and Dynamics of Membranes,* edited by R. Lipowsky and E. Sackmann (Elsevier, Amsterdam, 1994), Vol. 1; A. Zilker, M. Ziegler, and E. Sackmann, Phys. Rev. A **46**, 7998 (1992).

[4] M. Mutz and W. Helfrich, Phys. Rev. Lett. **62**, 2881

(1989).
[5] M. B. Schneider, J. T. Jenkins, and W. W. Webb, J. Phys. (Paris) **45**, 1457 (1984).
[6] S. T. Milner and S. A. Safran, Phys. Rev. A **36**, 4371 (1987).
[7] H. P. Duwe and E. Sackmann, Physica A **163**, 410 (1990).
[8] J. F. Faucon, M. D. Mitov, P. Meleard, I. Bivas, and P. Bothorel, J. Phys. (Paris) **50**, 2389 (1989).
[9] C. Safinya, D. Roux, G. S. Smith, S. K. Sinha, P. Dimon, N. A. Clark, and A. M. Bellocq, Phys. Rev. Lett. **57**, 2718 (1986); C. R. Safinya, E. B. Sirota, D. Roux, and G. S. Smith, *ibid.* **62**, 1134 (1989).
[10] R. M. Servuss and W. Helfrich J. Phys. (Paris) **50**, 809 (1989).
[11] E. Evans and V. A. Parsegian, Ann. N.Y. Acad. Sci. **416**, 13 (1983); E. Evans and M. Metcalfe, Biophys. J. **46**, 423 (1984); E. Evans and W. Rawicz, Phys. Rev. Lett. **64**, 2094 (1990).
[12] S. M. Bailey, S. Chiruvolu, J. N. Israelachvili, and J. A. N. Zasadzinski, Langmuir **6**, 1326 (1990).
[13] J. Rädler and E. Sackmann, J. Phys. (France) II **3**, 727 (1993).
[14] U. Seifert and R. Lipowsky, Phys. Rev. A **42**, 4768 (1990); K. Berndl, J. Käs, R. Lipowsky, E. Sackmann, and U. Seifert, Europhys. Lett. **13**, 659 (1990); L. Miao, B. Fourcade, M. Rao, and M. Wortis, Phys. Rev. A **43**, 6843 (1991).
[15] J. N. Israelachvili, *Intermolecular and Surface Forces* (Academic, London, 1991).
[16] J. Mahanty and B. W. Ninham, *Dispersion Forces* (Academic, London, 1976).
[17] R. Lipowsky, in *Structure and Dynamics of Membranes,* [3].
[18] R. Lipowsky and S. Leibler, Phys. Rev. Lett. **56**, 2541 (1986).
[19] W. Helfrich and R.-M. Servuss, Nuovo Cimento D **3**, 137 (1984).
[20] R. Lipowsky and B. Zielinska, Phys. Rev. Lett. **62**, 1572 (1989).
[21] W. Janke and H. Kleinert, Phys. Rev. Let. **58**, 144 (1987).
[22] G. Gompper and D. M. Kroll, Europhys. Lett. **9**, 59 (1989).
[23] R. Podgornik and V. A. Parsegian, Langmuir **8**, 557 (1992).
[24] R. Netz, Phys. Rev. E **51**, 2286 (1995).
[25] R. Netz and R. Lipowsky, Europhys. Lett. (to be published).
[26] S. Grotehans and R. Lipowsky, Phys. Rev. A **41**, 4575 (1990).
[27] W. Helfrich, in *Phase Transitions in Soft Condensed Matter,* edited by T. Riste and D. Sherrington (Plenum, New York, 1989), p. 271.
[28] E. Evans, Langmuir **7**, 1900 (1991).
[29] R. M. A. Azzam and N. M. Bashara, *Ellipsometrie and Polarized Light* (North-Holland, Amsterdam, 1975).
[30] M. I. Angelowa and D. S. Dimitrow, Mol. Cryst. Liq. Cryst. **152**, 89 (1987).

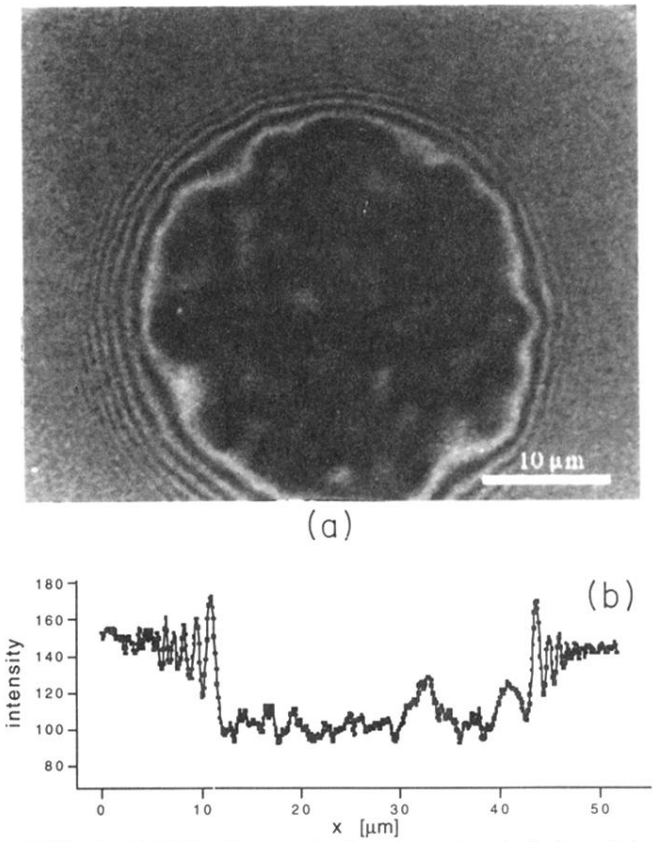

FIG. 4. (a) RIC micrograph of a giant phospholipid vesicle above a BSA coated MgF_2 substrate. The fringes at the edge of the round contact area arise from the up-bending profile. (b) Intensity scan through center of contact area. The momentary intensity of one frame reflects the distorted contour of the membrane by thermal fluctuations.